IEEE Access
Multidisciplinary | Rapid Review | Open Access Journal

Received March 24, 2019, accepted March 29, 2019, date of publication April 2, 2019, date of current version April 16, 2019.

Digital Object Identifier 10.1109/ACCESS.2019.2908866

Foreign Object Detection in a Wireless Power Transfer System Using Symmetrical Coil Sets

LIJUAN XIANG, ZE ZHU, JINDONG TIAN, AND YONG TIAN

Key Laboratory of Optoelectronic Devices and Systems of Ministry of Education and Guangdong Province, College of Physics and Optoelectronic Engineering, Shenzhen University, Shenzhen 518060, China

Corresponding author: Yong Tian (ytian@szu.edu.cn)

This work was supported in part by the National Natural Science Foundation of China under Grant 61803268, and in part by the Science and Technology Plan Project of Shenzhen under Grant JCYJ20170412110241478.

ABSTRACT In this paper, a foreign object detection (FOD) method based on symmetrical coil sets is proposed to prevent wireless power transfer (WPT) systems from heating, which could possibly cause an accidental fire. First, the influence of a foreign metal object on the magnetic field distribution of the WPT system is analyzed. Then, a two-layer symmetrical detection coil set is proposed considering the magnetic field characteristics. This kind of FOD method can reduce the design complexity, and the detection strategy is easily realized. The mutual inductance variation patterns are used to detect the presence and location of metal objects. Four scenarios of foreign object intrusion, including one coin with different locations, a coin on top of two adjacent detection coils with the same cover area, different test bodies, and different numbers of coins, are taken into consideration for validating the effectiveness of the proposed FOD method. Finally, a WPT system prototype with symmetrical coil sets for FOD detection is established. Both the simulation and experimental results indicate that the proposed method can effectively detect the presence and location of foreign objects.

INDEX TERMS Wireless power transfer, symmetrical coil sets, foreign object detection, heating effect.

I. INTRODUCTION

A wireless power transfer (WPT) system can transfer electrical power from the grid to electrical loads without any wired connections [1]. In the past few decades, many research institutes and scholars have delved into WPT technology for electric vehicles (EVs) [2]–[13]. At the same time, many companies have paid attention to its commercialization to accelerate the practical application of this technology. In the process, there is an urgent need to solve various problems. Among them, foreign object detection (FOD), especially metal object detection (MOD), is one of the most important issues facing WPT systems [14]. A WPT system must detect foreign objects when a foreign object is located in the operational area (i.e., the charging zone) between the transmitter coil and receiver coil. Because the temperature of a foreign object will rise according to its magnetic permeability, especially when the object is combined with a low-ignition point object, there is a high risk of fire. Accordingly, FOD is an important issue for WPT systems in practice to ensure operational safety.

The associate editor coordinating the review of this manuscript and approving it for publication was Emanuele Crisostomi.

The techniques for FOD have also been discussed in standards groups such as the Society of Automotive Engineers (SAE) and the International Electrotechnical Commission (IEC). The SAE has issued wireless power transfer standards such as the SAE J2954 Standard for Light-Duty Plug-In/Electric Vehicles and Alignment Methodology. Thirteen foreign bodies are required to be tested in the SAE J2954^{TM} November 2017 version, including a paper clip, staple, coin, nail, beverage can, steel sheet, etc. [15]. Similarly, the test bodies are also specified in the IEC 61980-3 Standard [16]. In the IEC standard, the size and material of the test objects are basically the same as the foreign matter types in the SAE standard. These test objects are deemed to have sufficient heat capacity to cause a fire by burning themselves or surrounding flammable objects. In addition, the overheating objects could scald people who touch them. Accordingly, aiming to address safety concerns, a dependable technique to detect foreign objects must be implemented in WPT systems.

To prevent foreign object combustion due to a temperature rise in the WPT system, various FOD methods have been developed [17]–[23]. A method based on detecting the system parameters, such as the voltage and current phase of the

transmitter coil, and the impedance characteristics was proposed in [17], [18]. Sensor techniques, such as temperature sensors can also be adopted in this scenario [19]. Comparing the power loss with and without foreign bodies is another option [20]. A basic FOD method is to place several additional coils between the transmitter coil and receiver coil, in which the magnetic field distribution is different with and without foreign objects [21], [22]. Among these solutions, the FOD method based on magnetic field distribution may be the best candidate for practical application, because it is easily realized and has a simple and effective structure. In Ref [22], dual-purpose non-overlapping coil sets were proposed to detect metal objects. It can detect the presence of foreign object and the EV position simultaneously by measuring the induced voltage difference of the coil sets. This method suffers from the dilemma of a dead zone, so another coil layer, non-overlapped with the first one, has to be added. In addition, the geometrical structure of the coil sets is relatively complex.

Instead of using the voltage difference between adjacent detection coils with and without the presence of a foreign object, the presented method in this paper utilizes the voltage differences between each symmetrical detection coil set to detect the position of foreign objects. The magnetic field generated by the transmitter coil forms a symmetrical distribution in both the horizontal and vertical directions. Thus, the induced voltages of two detection coils which are aligned symmetrically are assumed to be equal in the absence of foreign objects. As a result, with the intrusion of a foreign object, the voltage changes can be predicted with good accuracy. This method also reduces the design complexity because simple rectangular detection coils are used.

This paper is organized as follows, Section I provides the research background of FOD and the structure of the paper. In Section II, the FOD function considerations are presented, and the design of a FOD system is illustrated. Section III gives the model using ANSYS MAXWELL software, and the mutual inductance results considering different locations of the coin selected as the foreign object are presented. Additionally, three more scenarios, including different test materials and object quantities, are presented to verify the effectiveness of the proposed FOD method. An experimental prototype is established to further prove the feasibility of the proposed detection method in Section IV. Finally, the paper is summarized in Section V.

II. FOREIGN OBJECT DETECTION METHODOLOGY

A. DESIGN CONSIDERATIONS

A foreign object is likely to be located within the air gap between the transmitter coil and receiver coil in a WPT system. Among all kinds of objects, the power transfer efficiency and operation safety of the WPT system can be severely affected by metal materials. In addition, foreign objects may cause excessive temperatures that could become a touch hazard or fire issue.

In EV wireless charging applications, the transmitter coil is buried underground, and the receiver coil is attached to the vehicle chassis. The charging zone can be defined as the air space between the ground and the chassis. The influence of a metal object intrusion in the charging zone can be summarized as the temperature rise, the magnetic effect, and the eddy current effect. In this paper, we focus on the non-ferromagnetic objects, so the eddy current effect is analyzed.

The effects of the eddy current are analyzed in two aspects, one is the magnetic field, and the other is the impedance characteristic of the transmitter coil. Fig. 1 shows the schematic diagram of the eddy current.

Fig. 1 indicates that as the magnetic field, H_1, generated by the excitation current, I_1, goes through the metal area, induced electromotive force (EMF) will be generated in such way to produce the current, I_2, inside the metal. I_2 is ring-shaped, and it is defined as eddy current. Then, a new magnetic field, H_2, will be generated by I_2, and it will oppose the change of the original field, H_1.

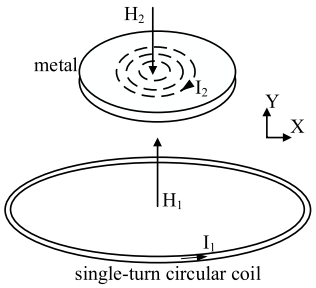

FIGURE 1. Schematic diagram of the eddy current.

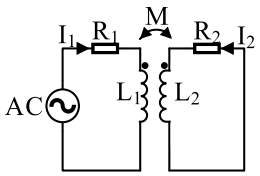

FIGURE 2. Equivalent circuit with a foreign object.

Moreover, the impedance characteristic of the transmitter coil will be influenced by the eddy current in the metal. The equivalent circuit of the transmitter coil and a foreign object is presented in Fig. 2, where AC is the equivalent source of the circuit, L_1 and R_1 are the inductance and resistance of the transmitter coil, respectively, L_2 and R_2 represent inductance and resistance of the foreign object, respectively. M is the mutual inductance between the transmitter coil and the foreign object. I_1 is the transmitter current and I_2 is the induced current.

Without foreign objects, the impedance of the transmitter coil can be expressed as:

$$Z_1 = R_1 + j\omega L_1 \tag{1}$$

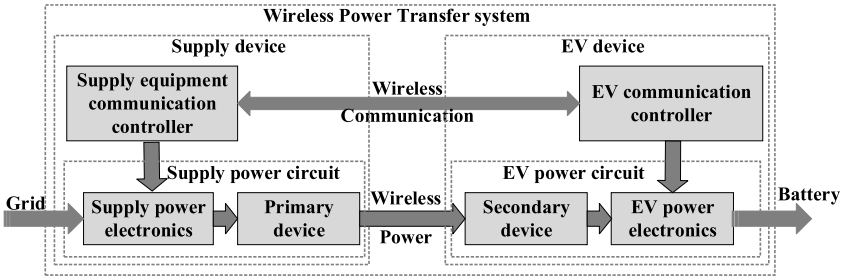

FIGURE 3. Schematic of a WPT system for EVs.

According to Kirchhoff's voltage law (KVL) theory, we have:

$$\begin{cases} R_1\dot{I}_1 + j\omega L_1\dot{I}_1 - j\omega M\dot{I}_2 = U \\ R_2\dot{I}_2 + j\omega L_2\dot{I}_2 - j\omega M\dot{I}_1 = 0 \end{cases} \tag{2}$$

According to (2), the total impedance from the transmitter coil can be revised as:

$$Z_1' = R_1' + j\omega L_1' \tag{3}$$

where

$$\begin{cases} R_1' = R_1 + \dfrac{\omega^2 M^2}{R_2^2 + \omega^2 L_2^2} R_2 \\ L_1' = L_1 - \dfrac{\omega^2 M^2}{R_2^2 + \omega^2 L_2^2} L_2 \end{cases} \tag{4}$$

By comparing (1) and (4), it is clear that the equivalent resistance of the total impedance increases and the inductance decreases due to the eddy current. Thus, the foreign object will influence the impedance characteristic, as well as the system charging performance.

As shown in Fig. 1, magnetic flux is generated at the coil when the current flows. While a foreign object with area, S, is placed along the Y-axis, which is parallel to the coil, the portion of magnetic flux, Φ, linking the foreign object can be written as:

$$\Phi = \int_S B \cdot dS \tag{5}$$

where B is the magnetic field strength at the metal area.

The mutual inductance between the transmitter coil and the foreign object is:

$$M = \frac{\Phi}{I_2} = \frac{\int_S B \cdot dS}{I_2} \tag{6}$$

The induced voltage in the foreign object generated by the transmitter coil can be expressed as:

$$U' = \omega M I_1 \tag{7}$$

From the above analysis, the operation of the WPT system is highly affected by the eddy current of metal objects. Therefore, this paper focuses on the metal object detection.

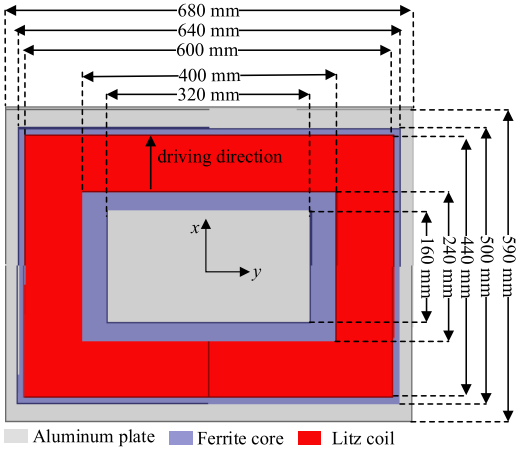

FIGURE 4. Mechanical dimensions of the transmitter coil.

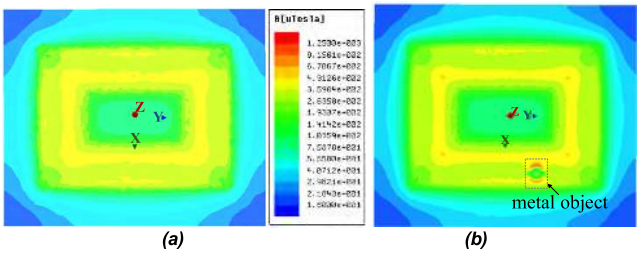

FIGURE 5. Distribution of the magnetic field strength (a) without a foreign object, (b) with a foreign object.

An example of the WPT system for electric vehicle charging is illustrated in Fig. 3. It mainly includes two parts, namely, the supply device and on-board (EV) device. In general, the Litz coils with specific configurations should be used as the key part of both the primary and secondary devices in order to reduce the skin effect of high-frequency current.

As an example, Fig. 4 shows the mechanical dimensions of a typical transmitter coil (primary coil) according to the SAE J2954^{TM} Nov2017 version. The magnetic field strength distribution of the transmitter coil without and with a foreign object is presented in Fig. 5. In the simulation, the excitation current of the transmitter coil is set as 10 A.

From Fig. 5(a), it is seen that the magnetic field is symmetrically distributed along both the X and Y axes. Fortunately, the magnetic field distribution of the reference

primary devices proposed in the SAE, IEC and ISO standards and other conventional coils is also essentially symmetrical. As illustrated in Fig. 5(b), when a foreign object is placed in the charging zone, the value of the magnetic strength, B, changes, and reaches the peak on the surface of the foreign object. The maximum values of these two scenarios are quite different. The value without a foreign object is 523 μT in Fig. 5(a), while the value with a foreign object is 1241 μT in Fig. 5(b). It is possible to confirm that these changes of the magnetic flux are the cause of fire and other safety concerns.

B. PROPOSED DETECTION COIL SETS

Considering the characteristic of the above magnetic field distribution, a symmetrical configuration for detection coil sets is proposed in this paper. Coil winding, as well as the structures of the primary device and secondary device, are illustrated in Fig. 6.

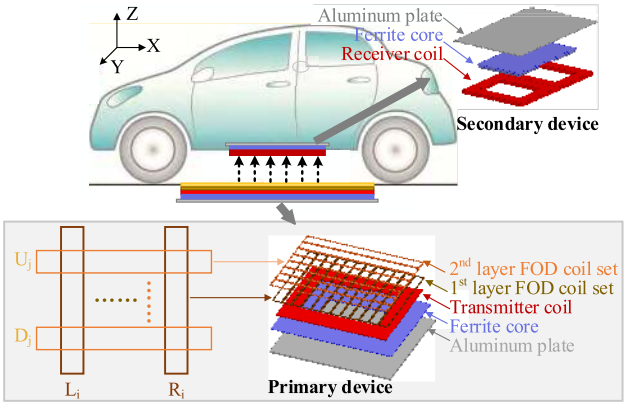

FIGURE 6. Proposed coil set configuration.

In Fig. 6, there are two layers of detection coils for accurately detecting the location of foreign objects. n coils are arranged along with the Y-axis on the first layer, and m coils are arranged along the X-axis on the second layer. Two symmetrical rectangles located on the two sides comprise one coil set, and the area of each rectangle meets the condition:

$$\begin{cases} S_{L_i} = S_{R_i}, & i = 1, \ldots, n \\ S_{U_j} = S_{D_j}, & j = 1, \ldots, m \end{cases} \tag{8}$$

where the subscript L represents the coil on the left side, R is the coil on the right side, U is the upper coil, and D is the lower coil.

The detection strategy with the proposed symmetrical coil sets is summarized as follows: without the foreign objects, the magnetic field strength generated by the transmitter coil passing through cross-section of the two symmetrically distributed areas of detection coils have the same values, but the magnetic field directions are opposite. This characteristic will be changed when a foreign object is placed on top of the primary device.

According to (7), the induced voltage is proportional to the mutual inductance. The foreign objects can be detected by evaluating the induced voltages. It should be noted that the directions of the coils in the two layers are different. With such a winding structure, it not only detects the voltage difference in the coil sets to verify the existence of foreign materials, but also obtains the location.

The mutual inductance, M, in (7) can be expressed as:

$$\begin{cases} |\Delta M_i| = ||M(L_i, P)| - |M(R_i, P)||, & 1^{\text{st}}\text{layer} \\ |\Delta M_j| = \big||M(U_j, P)| - |M(D_j, P)|\big|, & 2^{\text{nd}}\text{layer} \end{cases} \tag{9}$$

where $M(\mathrm{L_i}, \mathrm{P})$ represents the mutual inductance between the left-hand detection coils and the primary coil, $M(\mathrm{R_i}, \mathrm{P})$ represents the mutual inductance with the detection coils on the right side, $M(\mathrm{U_j}, \mathrm{P})$ and $M(\mathrm{D_j}, \mathrm{P})$ represent the mutual inductance between the coils on the second layer and the primary coil, respectively. $|\triangle M_\mathrm{i}|$ is the equivalent mutual inductance difference of the i^{th} coil set.

In this study, the FOD method is based on the calculation of the induced voltage difference of the two symmetrical detection coils. Therefore, detecting the change in mutual inductance to determine whether foreign objects exist or not is also effective. The FOD can be accomplished by analyzing the detection results.

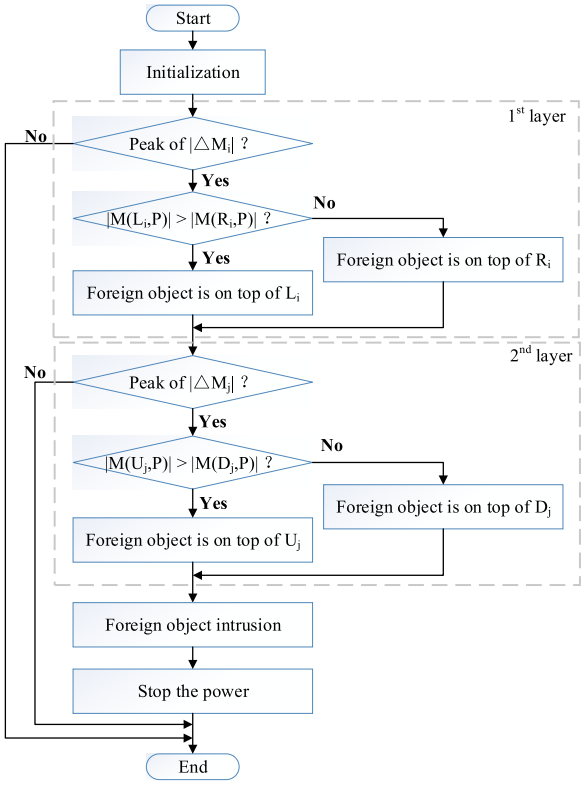

FIGURE 7. Flowchart of the proposed FOD method.

C. FOD PROCEDURE

Based on the above discussion, the proposed FOD method is explained by the flowchart in Fig. 7. The presence and location of the foreign objects can be determined according to the patterns of all the M, $|\triangle M_i|$ and $|\triangle M_j|$ values.

For example, if there exists a peak among the $|\triangle M_i|$ values, a foreign object intrusion has occurred in the charging zone. The number of peaks indicates the quantity of foreign objects. One peak among $|\triangle M_i|$ values means that one foreign object exists in the charging zone, and the subscript i represents that the foreign object is located on the i^{th} detection coil set. Furthermore, the location of the foreign object can be determined by comparing $|M(\mathrm{L_i}, \mathrm{P})|$ with $|M(\mathrm{R_i}, \mathrm{P})|$. If two points contribute to the peak $|\triangle M_i|$, it is indicated that the foreign object covers two adjacent detection coils. Otherwise, the foreign object is located on top of a single detection coil.

Fig. 7 illustrates the FOD process with the M and $|\triangle M|$ patterns. The idea is that the mutual inductance values can be directly derived according to the simulation model in the ANSYS MAXWELL software. Moreover, the induced voltage is proportional to the mutual inductance, as shown in (7). The induced voltage differences of the symmetrical coil sets will be used as the detection criterion in the experiments, because in practice, they can be easily measured online as compared with the mutual inductance.

As shown in Fig. 7, the presence and location of foreign objects can be detected as follows: First, the presence of foreign objects is detected according to the $|\triangle M_i|$, $|M(\mathrm{L_i}, \mathrm{P})|$, and $|M(\mathrm{R_i}, \mathrm{P})|$ values. It is indicated that the foreign object is located on the i^{th} detection coil set when $|\triangle M_i|$ has the maximum value. Then, the horizontal location of the foreign object is further determined by comparing $|M(\mathrm{L_i}, \mathrm{P})|$, and $|M(\mathrm{R_i}, \mathrm{P})|$. The foreign object is located on top of coil $\mathrm{L_i}$ if the value of $|M(\mathrm{L_i}, \mathrm{P})|$ is larger than the value of $|M(\mathrm{R_i}, \mathrm{P})|$. Otherwise, the foreign object is located on top of coil $\mathrm{R_i}$. Thus, the position of the foreign object along the Y-axis can be detected. Similarly, the vertical location of the foreign object can be further determined with the detection coils on the second layer. Hence, both the presence and location of the foreign objects can be determined using the proposed detection coil sets. Generally, the proposed FOD method works by recognizing the mutual inductance difference patterns of the detection coils caused by foreign objects. The location difference of the foreign objects could cause a different peak response of the mutual inductance difference.

III. SIMULATION VALIDATION FOR FOD DETECTION

A. SIMULATION MODEL

In this section, a simulation model with detection coils is designed, as presented in Fig. 8. In the simulation, six pairs of coils arranged in the horizontal direction on the first layer, i.e., $\mathrm{L_1}, \mathrm{L_2}, \ldots, \mathrm{L_6}, \mathrm{R_6}, \ldots, \mathrm{R_2}, \mathrm{R_1}$ (named as lateral detection coils), and four pairs of coils arranged in the vertical direction on the second layer, i.e., $\mathrm{U_1}, \ldots, \mathrm{U_4}, \mathrm{D_4}, \ldots, \mathrm{D_1}$ (named as vertical detection coils), are used to determine the feasibility of the model. The parameters for the primary device, detection coils and the foreign object are listed in Table 1. A coin with a radius of 15 mm and a height of 2 mm is used as the test object.

The mutual inductance values between the lateral detection coils and the transmitter coil are presented in Fig. 9 for the initial condition, without any coin on top of the primary device. It can be seen that on the first layer, M values of coils on the left side are negative and the absolute values are the same as the relevant ones on the right side. This reveals that the mutual inductance difference, $|\triangle M_i|$, of the two coils in one detection coil set is equal to zero.

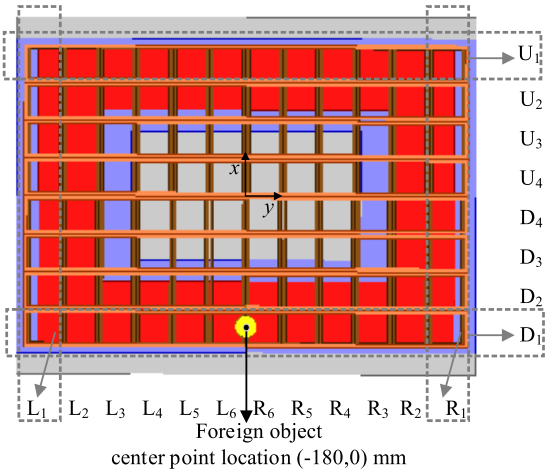

FIGURE 8. Simulation model for FOD.

TABLE 1. Simulation parameters.

Parameters	Values
Aluminum plate size	680*590*40 mm^3
Ferrite core size	640*500*3 mm^3 (outer) 320*160*3 mm^3 (inner)
Primary Litz coil size	600*440*5 mm3 (outer) 580*420*5 mm3 (inner)
Primary coil turns	10
Primary coil current	30A
Horizontal detection coil size	50*440*2 mm^3 (outer) 48*438*2 mm^3 (inner)
Vertical detection coil size	600*52*2 mm^3 (outer) 598*50*2 mm^3 (inner)
Coin size	r=15 mm, h=2 mm

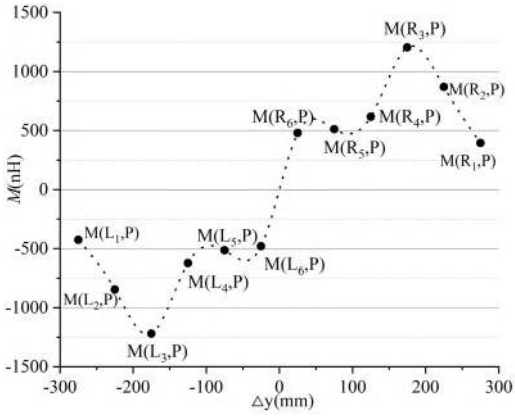

FIGURE 9. Mutual inductances between the detection coils and primary coil.

B. PERFORMANCE ANALYSIS

A coin is placed on top of the primary device, as presented in Fig. 8. The initial center point of the coin along the X-axis is −180 mm, and the value along the Y-axis is 0 mm. All the mutual inductance values change with the changing placement of the coin. To evaluate the variation characteristics of $M(\mathrm{L_i}, \mathrm{P})$ and $M(\mathrm{R_i}, \mathrm{P})$, the position of the coin is parameterized, and the moving distance of the coin along the Y-axis is defined as $\triangle y$. Herein, $\triangle y$ is set to be varied from −275 mm to 275 mm in steps of 50 mm. The simulation results for the mutual inductance, M, are shown in Fig. 10.

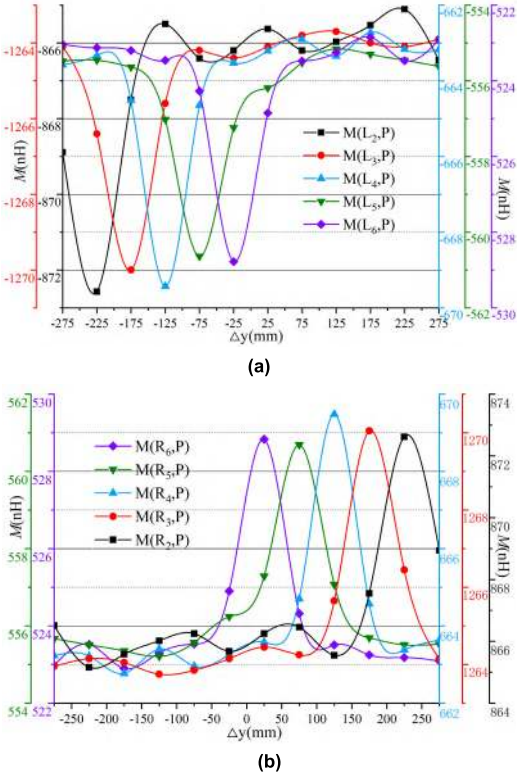

FIGURE 10. M simulation results with different |△y| values. (a) M(L_i, P). (b) M(R_i, P).

As seen in Fig. 10, all the M values vary with the different locations of the coin. When the coin is placed on top of a detection coil, the relevant M reaches the peak value. For example, the initial value of $M(\mathrm{L_3}, \mathrm{P})$ is approximately −1220.9 nH, as shown in Fig. 9. In Fig. 10(a), the solid red curve represents the $M(\mathrm{L_3}, \mathrm{P})$ with a range of [−1270, −1264] nH. When the center point of the coin is at the location $\triangle y = -175$ mm, meaning the coin is on top of detection coil $\mathrm{L_3}$, it is found that $M(\mathrm{L_3}, \mathrm{P})$ has the maximum value of −1270 nH. Compared with its initial value of −1220.9 nH, $M(\mathrm{L_3}, \mathrm{P})$ has a variation of 49.1 nH.

By substituting the simulation values presented in Fig. 10 into (9), the variation curves of $|\triangle M_i|$ can be obtained as shown in Fig. 11.

It can be seen from Fig. 11 that the variation of $|\triangle M_i|$ is similar to that of $M(\mathrm{L_i}, \mathrm{P})$ and $M(\mathrm{R_i}, \mathrm{P})$. Therefore, the coin

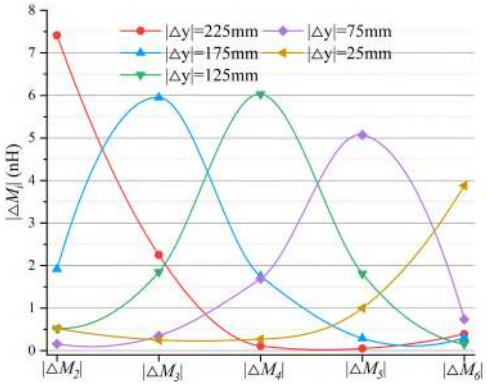

FIGURE 11. $|\triangle M_i|$ values with different $|\triangle y|$ values.

can be detected by evaluating the mutual inductance variation patterns. For example, the solid blue curve in Fig. 11 indicates that the coin is located on top of the third coil set ($|\triangle y| = 175$ mm), because $|\triangle M_3|$ has the maximum value among all the $|\triangle M_i|$. Furthermore, based on the solid red curves in Fig. 10, the values of $M(\mathrm{L_3}, \mathrm{P})$ and $M(\mathrm{R_3}, \mathrm{P})$ are −1270 nH and 1264.05 nH respectively. Then, we have $|M(\mathrm{L_3}, \mathrm{P})| > |M(\mathrm{R_3}, \mathrm{P})|$, which indicates that the coin is located on top of coil $\mathrm{L_3}$ according to the detection criterion in Fig. 7.

C. FURTHER VERIFICATION

The existing FOD methods might suffer from a dead zone situation [20]. More details about this will be introduced in this section. To further validate the effectiveness of the proposed method, three more scenarios of foreign object intrusion are taken into consideration.

For example, the initial location of the coin, as shown in Fig. 8, is (−180, 0) mm. The coin is symmetrically located on top of detection coils $\mathrm{L_6}$ and $\mathrm{R_6}$, meaning that it covers the same area on both $\mathrm{L_6}$ and $\mathrm{R_6}$.

The simulation sweep parameter is set as follows, $\triangle y$ varies from −250 mm to 250 mm in steps of 50 mm. To simplify the simulation, only two detection coil sets on the first layer are adopted in this scenario. The $M(\mathrm{L_i}, \mathrm{P})$, $M(\mathrm{R_i}, \mathrm{P})$, and $|\triangle M_i|$ values of $i = 4, 5$ are given in Fig. 12.

From Fig. 12(a), it is clear that all the M curves present peaks, and there are two adjacent points with high values. In Fig. 12(b), the fourth detection coil set has the peak of $|\triangle M_4|$ on $|\triangle y| = 100$ mm and 150 mm, additionally, $|\triangle M_5|$ has the peak of $|\triangle y| = 50$ mm and 100 mm.

According to Figs. 10-12, the M and $|\triangle M_i|$ of this scenario have similar variation patterns in the first scenario. Moreover, when the coin is placed on top of two adjacent detection coils with the same cover area, the curves have the peaks at two points. This phenomenon is different from the first one, which means that the proposed method can detect the foreign object even when it covers two adjacent detection coils.

Furthermore, as discussed in Section I, 15 types of test bodies are listed in Table 309 in IEC 61980-3 Standard, and the simulation with two different test bodies will be discussed. The parameters are listed in Table 2.

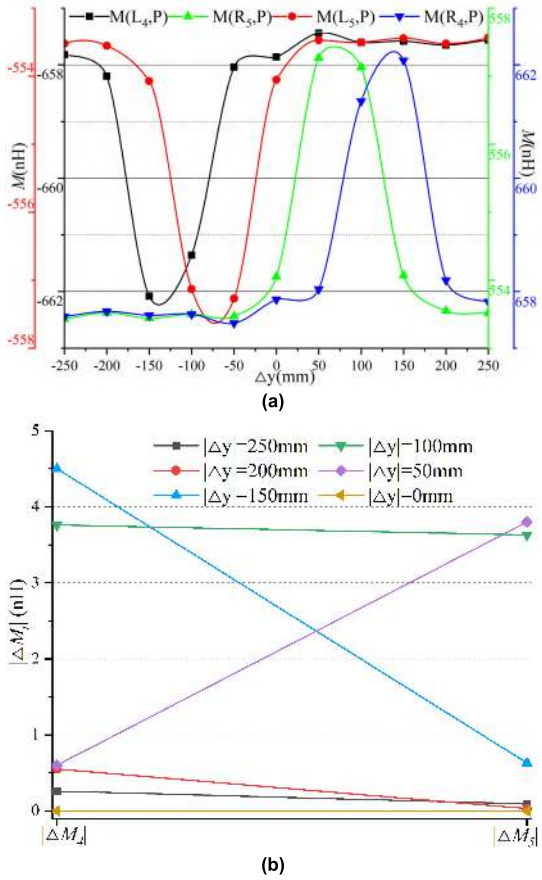

FIGURE 12. The *M and* $|\triangle M_i|$ simulation results with different $|\triangle y|$ values. (a) M variation curves. (b) $|\triangle M_i|$ variation curves.

TABLE 2. Test objects.

Label	Object	Size	Material
#1	Solid steel disc	r=20 mm, h=1.5 mm	Steel
#2	Coin	r=15 mm, h=2 mm	Fe

To simplify the simulation, only one detection coil set, L_4 and R_4 is adopted in this model. The simulation results are illustrated in Fig. 13 and Table 3.

From Fig. 13, it is seen that the simulation results for mutual inductance under this scenario performs similarly to that of the first scenario. The value ranges are dependent on the size and material of the foreign objects. In Table 3, $|\triangle M_4|$ has the maximum value at $|\triangle y| = 100$ mm regardless of the test objects. It indicates that both test objects can be detected using the proposed FOD method.

In addition, the scenario of more than one foreign object in the charging zone is considered herein. Fig. 14 depicts the simulation results with two objects at two different locations. It is clear that both black and red solid curves have two peaks. For example, when two coins are placed on top of L_4 and R_2, a peak is simultaneously found in $|\triangle M_2|$ and $|\triangle M_4|$.

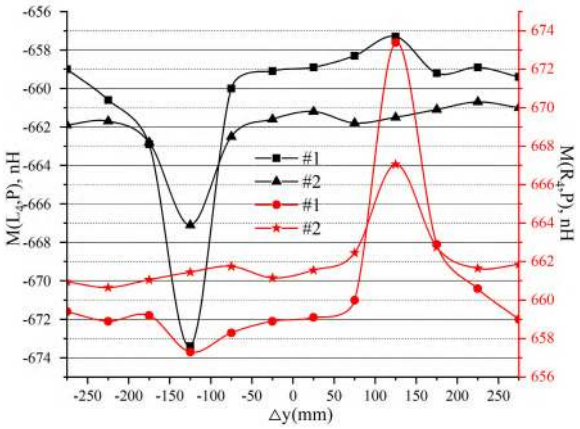

FIGURE 13. *M* simulation results for different test objects.

This characteristic can be used as the detection strategy with more than one foreign object scenario.

IV. EXPERIMENTAL VERIFICATION

A. EXPERIMENTAL CONFIGURATION

An experimental prototype as shown in Fig. 15 is established to confirm the practicality of the proposed FOD method. The primary LCC compensation topology is selected considering the constant current characteristic of transmitter coil [24]. The detection coils are fabricated on a printed circuit board (PCB). The top layer with four detection coil sets is tested herein. The detection coils are labeled as L_1, L_2, L_3, L_4, R_4, R_3, R_2, and R_1. Parameters of the WPT system prototype are listed in Table 4.

It is found that the original magnetic field generated by the transmitter coil has a very small difference even at the symmetrical locations due to the manual winding error of the transmitter coil. Therefore, a variable resistor is designed to adjust the initial induced voltage without the foreign object. The variable resistor is parallel to the output voltage. The block diagram of this prototype is shown in Fig. 16.

B. EXPERIMENTAL RESULTS AND DISCUSSION

Referring to Equation (7), the induced voltage of the detection coil is positively proportional to mutual inductance, M. Therefore, the induced voltages of the detection coils in the prototype are used as our measuring variables to test the proposed FOD method. The Chinese coins (one Yuan) with a 25 mm diameter are used as the foreign objects. Fig. 17 depicts the induced voltages of the two detection coil sets. The voltages of L_2, R_2, L_3, and R_3 are measured by channel 1, 2, 3 and 4, respectively.

Fig. 17(a) plots the voltage waveforms without the coins, and it can be seen that the initial voltages of the second coil set are both 666 mV, meanwhile, the values of the third coil are both 662 mV. It is noted that the induced voltages of two symmetrical coils in a coil set have the same values. The voltages with different locations of FOD, including a single coin located on top of L_2, a single coin located on the top of L_3,

TABLE 3. $|\triangle M_4|$ results with different coin locations.

$\lvert\triangle M_4\rvert$(nH)	$\lvert\triangle y\rvert$=250 mm	$\lvert\triangle y\rvert$=200 mm	$\lvert\triangle y\rvert$=150 mm	$\lvert\triangle y\rvert$=100 mm	$\lvert\triangle y\rvert$=50 mm	$\lvert\triangle y\rvert$=0
#1 test object	0.4	1.7	3.7	16.1	1.7	0.2
#2 test object	0.95	1.1	1.7	5.7	0.75	0.4

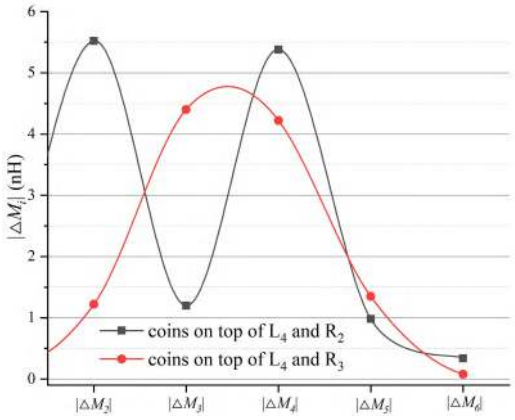

FIGURE 14. The $|\triangle M_i|$ simulation results with two coins.

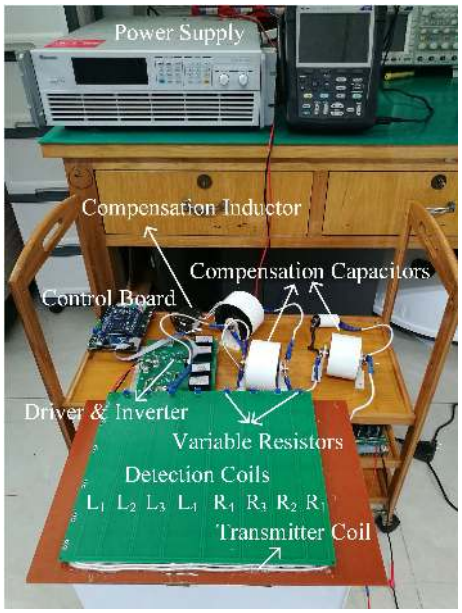

FIGURE 15. WPT system prototype with the FOD function.

TABLE 4. Specification of the WPT system prototype.

Parameter	Value
Operating frequency	86.6 kHz
Input voltage	40 V
Transmitter current	6 A
Variable resistor	[0, 50000] Ω
Transmitter coil size	330*270*5 mm^3(outer) 250*190*5 mm^3(inner)
Transmitter coil winding number	9 turns
Transmitter coil inductance	50 μH
Primary capacitor	0.09 μF
Compensative inductor	11 μH
Compensative capacitor	0.32 μF

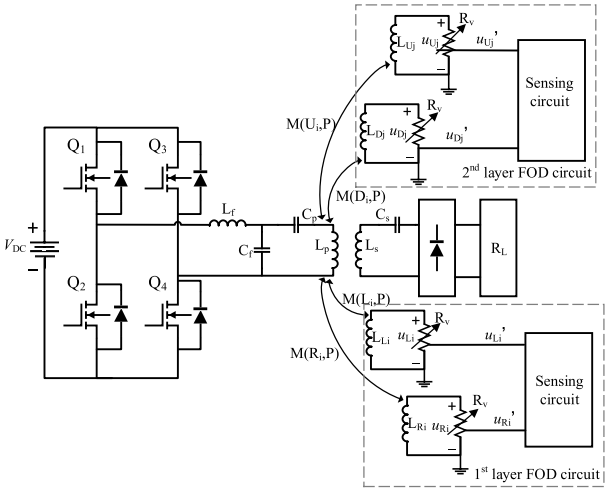

FIGURE 16. Circuit diagram of the WPT prototype with FOD.

and two coins symmetrically located on top of L_2 and L_3, are shown in Fig. 17(b)-(d). In Fig. 17(b), the variation values of the coil sets (L_2, R_2) and (L_3, R_3) are 6 mV and 1 mV, which means that the coin is located on the coil set (L_2, R_2). Additionally, the induced voltage of coil L_2 changes more than that of coil R_2, i.e., increasing from 666 mV to 672 mV. Based on the proposed detection criterion, the foreign object can be determined to be located on top of coil L_2. It is worth mentioning that the slight change of voltage difference of the coil sets without foreign objects, for example, (L_3, R_3), is caused by system noise and measurement error. Similarly, as shown in Fig. 17(c), when the coin is located on top of L_3, the L_3 voltage increases significantly, from 662 mV to 674 mV, while the other three values stay approximately the same in Fig. 17(a). In Fig. 17(d), the induced voltages of L_2 and L_3 increase from 666 mV to 672 mV and from 662 mV to 673 mV, respectively. These two values have a larger change than the other induced voltages, indicating that foreign objects are located on both L_2 and L_3. From the results shown in Fig. 17, it can be concluded that the foreign objects can be accurately detected even though they are located on top of two adjacent coils with the same cover area.

It should be mentioned that the level of inductance voltage difference in the coil sets is influenced by factors such as the

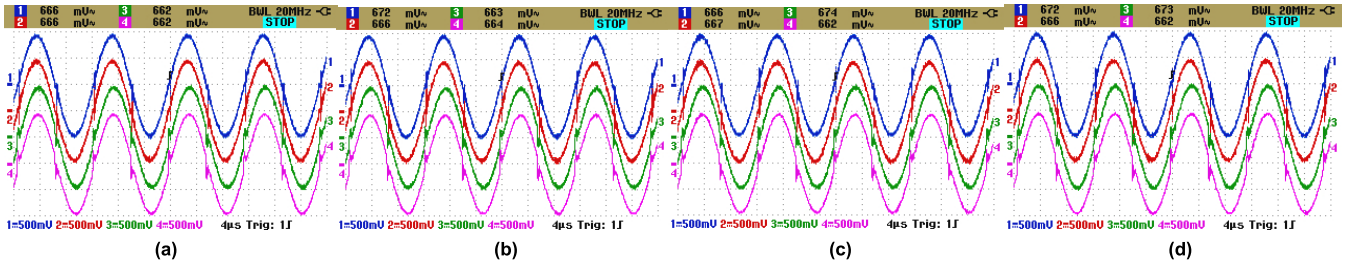

FIGURE 17. Induced voltage waveforms of the detection coils (a) without coins, (b) with a coin on top of L_2, (c) with a coin on top of L_3, (d) with a coin on top of L_2 and L3.

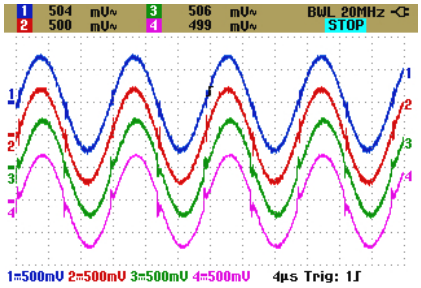

FIGURE 18. Induced voltage waveforms with two coins.

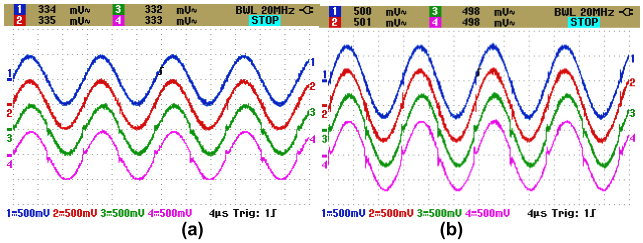

FIGURE 19. Induced voltage waveforms of detection coils (a) 20 V input voltage, (b) 30 V input voltage.

transmitter coil current, transmitter coil geometry, as well as the size and position of the detection coil. As an example, another test with two coins intrusion and a primary input voltage of 30 V (the transmitter coil current is 4.5 A) is performed, and the inductance voltage waveforms are shown in Fig. 18.

It is clear that the induced voltages of the four detection coils (L_2, R_2, L_3, and R_3) are 504 mV, 500 mV, 506 mV, and 499 mV, respectively. The voltage difference of coil set (L_2, R_2) is 4 mV and that of coil set (L_3, R_3) is 7 mV. Then, we conclude that two foreign objects exist in the WPT system because two peaks are detected among the voltage differences of all the coil sets. In a practical WPT system for EVs, the primary input voltage and transmitter coil current are both much larger than that of the prototype in this paper, which will cause a larger level of inductance voltage difference that can be detected more easily and robustly.

In addition, an experimental verification of the effectiveness of the variable resistor design is performed. The inductance voltage waveforms of the detection coil sets with different primary input voltages, including 20 V and 30 V are given in Fig. 19. According to Fig. 17(a) and Fig. 19, the inductance voltage values of two symmetrical coils can maintain the same values as the primary input voltage changes. Thus, it can be concluded that the inductance voltage difference of the symmetrical coil set caused by the manual winding error can be eliminated by using a variable resistor regardless of the primary input voltage.

V. CONCLUSIONS

This paper presented a foreign object detection method used in WPT system. Two-layer symmetrical detection coil sets are proposed to detect the presence and location of foreign objects. The symmetrical structure is designed considering the symmetrical distribution of the original magnetic field generated by the transmitter coil. The detection coils are designed with a rectangular geometry so that they are easily implemented in practice. Foreign objects can be detected by comparing the mutual inductance differences or induced voltage differences between two symmetrical coils, and accurately located by considering the results of the coil sets on the other layer. The simulation results under four typical scenarios using the ANSYS MAXWELL software provided the validation of the proposed method. A WPT system prototype is developed to further verify the proposed method. Four detection coil sets are fabricated on a PCB. The experimental results revealed that the proposed method can detect foreign objects regardless of their location and quantity. In addition, the designed variable resistor can effectively eliminate the initial voltage difference of two symmetrical coils caused by the winding error of the transmitter coil.

It is worth mentioning that, practical WPT systems, especially for those used in wireless EV charging, usually suffer from misalignment between the transmitter coil and receiver coil. It is possible to change the symmetry of the magnetic field generated by the transmitter coil. For this case, the foreign objects can be still detected with the symmetrical coil sets by using a correction algorithm, which will be introduced in our further work.

REFERENCES

[1] A. Kurs, A. Karalis, R. Moffatt, J. D. Joannopoulos, P. Fisher, and M. Solja ić, "Wireless power transfer via strongly coupled magnetic resonances," *Science*, vol. 317, no. 5834, pp. 83–86, 2007.

[2] C. C. Mi, G. Buja, S. Y. Choi, and C. T. Rim, "Modern advances in wireless power transfer systems for roadway powered electric vehicles," *IEEE Trans. Ind. Electron.*, vol. 63, no. 10, pp. 6533–6545, Oct. 2016.

[3] J. M. Miller, O. C. Onar, and M. Chinthavali, "Primary-side power flow control of wireless power transfer for electric vehicle charging," *IEEE J. Emerg. Sel. Topics Power Electron.*, vol. 3, no. 1, pp. 147–162, Mar. 2015.
[4] L. Zhao, D. Thrimawithana, and U. K. Madawala, "Hybrid bidirectional wireless EV charging system tolerant to pad misalignment," *IEEE Trans. Ind. Electron.*, vol. 64, no. 9, pp. 7079–7086, Sep. 2017.
[5] A. Ahmad, M. S. Alam, and R. Chabaan, "A comprehensive review of wireless charging technologies for electric vehicles," *IEEE Trans. Transport. Electrific.*, vol. 4, no. 1, pp. 38–63, Mar. 2018.
[6] Q. Deng *et al.*, "Edge position detection of on-line charged vehicles with segmental wireless power supply," *IEEE Trans. Veh. Technol.*, vol. 66, no. 5, pp. 3610–3621, May 2017.
[7] Y. Wang, Y. Yao, X. Liu, D. Xu, and L. Cai, "An LC/S compensation topology and coil design technique for wireless power transfer," *IEEE Trans. Power Electron.*, vol. 33, no. 3, pp. 2007–2025, Mar. 2018.
[8] C.-C. Huang, C.-L. Lin, and Y.-K. Wu, "Simultaneous wireless power/data transfer for electric vehicle charging," *IEEE Trans. Ind. Electron.*, vol. 64, no. 1, pp. 682–690, Jan. 2017.
[9] D. H. Tran, V. B. Vu, and W. Choi, "Design of a high-efficiency wireless power transfer system with intermediate coils for the on-board chargers of electric vehicles," *IEEE Trans. Power Electron.*, vol. 33, no. 1, pp. 175–187, Jan. 2018.
[10] A. A. S. Mohamed, A. A. Marim, and O. A. Mohammed, "Magnetic design considerations of bidirectional inductive wireless power transfer system for EV applications," *IEEE Trans. Magn.*, vol. 53, no. 6, pp. 1–5, Jun. 2017.
[11] L. Tan, S. Pan, H. Liu, C. Xu, J. Guo, and X. Huang, "Load detection method for multiple-receiver wireless power transfer systems," *IET Power Electron.*, vol. 10, no. 14, pp. 1951–1958, Nov. 2017.
[12] Z. Wang *et al.*, "A novel magnetic coupling mechanism for dynamic wireless charging system for electric vehicles," *IEEE Trans. Veh. Technol.*, vol. 67, no. 1, pp. 124–133, Jan. 2018.
[13] L. Xiang, X. Li, J. Tian, and Y. Tian, "A crossed DD geometry and its double-coil excitation method for electric vehicle dynamic wireless charging systems," *IEEE Access*, vol. 6, pp. 45120–45128, 2018.
[14] S. Y. R. Hui, "Technical and safety challenges in emerging trends of near-field wireless power transfer industrial guidelines," *IEEE Electromagn. Compat. Mag.*, vol. 7, no. 1, pp. 78–86, 1st Quart., 2018.
[15] *Wireless Power Transfer for Light-Duty Plug-In/Electric Vehicles and Alignment Methodology*, document SAE J2954TM, 2017.
[16] *Electric Vehicle Wireless Power Transfer (WPT) Systems—Part 3 Specific Requirements for the Magnetic Field Wireless Power Transfer Systems*, document IEC TS 61980-3, 2018.
[17] J. Pávó, Z. Badics, S. Bilicz, and S. Gyimóthy, "Efficient perturbation method for computing two-port parameter changes due to foreign objects for WPT systems," *IEEE Trans. Magn.*, vol. 54, no. 3, pp. 1–4, Mar. 2018.
[18] S.-J. Huang, J.-L. Su, S.-H. Dai, C.-C. Tai, and T.-S. Lee, "Enhancement of wireless power transmission with foreign-object detection considerations," *Proc. IEEE 6th Global Conf. Consum. Electron. (GCCE)*, Oct. 2017, pp. 1–2.
[19] C. K. Jung and B. U. Hwang, "Apparatus and method for detecting foreign object in wireless power transmitting system," U.S. Patent 20 140 232 199 A1, Aug. 8, 2014.
[20] N. Kuyvenhoven, C. Dean, J. Melton, J. Schwannecke, and A. E. Umenei, "Development of a foreign object detection and analysis method for wireless power systems," in *Proc. IEEE Symp. Product Compliance Eng.*, San Diego, CA, USA, Oct. 2011, pp. 1–6.
[21] S. Verghese, M. P. Kesler, K. L. Hall, and H. T. Lou, "Foreign object detection in wireless energy transfer systems," U.S. Patent 201 161 532 785 P, Sep. 9, 2011.
[22] S. Y. Jeong, H. G. Kwak, G. C. Jang, S. Y. Choi, and C. T. Rim, "Dual-purpose nonoverlapping coil sets as metal object and vehicle position detections for wireless stationary EV chargers," *IEEE Trans. Power Electron.*, vol. 33, no. 9, pp. 7387–7397, Sep. 2018.
[23] G. Ombach, "Design and safety considerations of interoperable wireless charging system for automotive," in *Proc. 9th Int. Conf. Ecological Vehicles Renew. Energies (EVER)*. Monaco: Monte-Carlo, Mar. 2014, pp. 1–4.
[24] S. Li, W. Li, J. Deng, T. D. Nguyen, and C. C. Mi, "A double-sided LCC compensation network and its tuning method for wireless power transfer," *IEEE Trans. Veh. Technol.*, vol. 64, no. 6, pp. 2261–2273, Jun. 2015.

LIJUAN XIANG received the B.S. degree in automation and the Ph.D. degree in control theory and control engineering from the College of Automation, Chongqing University, Chongqing, China, in 2012 and 2017, respectively.

From 2016 to 2017, she was a joint Ph.D. Student at The Pennsylvania State University, sponsored by the China Scholarship Council (CSC). She is currently a Postdoctoral Researcher with the College of Physics and Optoelectronic Engineering, Shenzhen University, China. Her research interests include electromagnetic field modeling and simulation, control theory and application, and wireless power transfer.

ZE ZHU was born in Jinan, Shandong, China, in 1995. He is currently pursuing the master's degree with Shenzhen University, Shenzhen, China.

JINDONG TIAN received the B.S. degree in precision machinery, the M.S. degree in optical instrument, and the Ph.D. degree in optical engineering from Tianjin University, Tianjin, China, in 1995, 1998, and 2001, respectively.

From 2001 to 2002, he was a Postdoctoral Researcher with the Department of Mechanical Engineering, The Hong Kong University of Science and Technology, China. He is currently a Professor with the College of Physics and Optoelectronic Engineering, Shenzhen University. His research interests include optical metrology, wireless power transfer, and lithium-ion battery management.

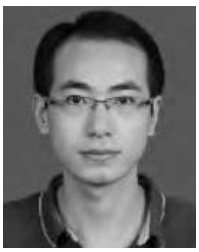

YONG TIAN received the B.S. degree in automation and the Ph.D. degree in control theory and control engineering from the College of Automation, Chongqing University, Chongqing, China, in 2008 and 2012, respectively.

From 2013 to 2015, he was a Postdoctoral Researcher with the Department of Mechanical Engineering, Tsinghua University, China. He is currently an Assistant Professor with the College of Physics and Optoelectronic Engineering, Shenzhen University. His research interests include wireless power transfer, computational and artificial intelligence, and lithium-ion battery management.